# Density Functional Theory Study of the Geometry, Energetics and Reconstruction Process of Si(111) Surfaces

*Santiago D. Solares*[a], *Siddharth Dasgupta*[a,b], *Peter A. Schultz*[c], *Yong-Hoon Kim*[a,d], *Charles B. Musgrave*[a,e] *and William A. Goddard III*[a*]

[a]Materials and Process Simulation Center, California Institute of Technology, Pasadena, CA, 91125

[b]Current address: Center for Neuromorphic Systems Engineering, California Institute of Technology, Pasadena, CA, 91125

[c]Multiscale Computational Materials Methods Department, Sandia National Laboratories, Albuquerque, NM 87185

[d]Current address: School of Computational Sciences, Korea Institute for Advanced Study, Seoul, 130-722 Korea

[e]Current address: Department of Chemical Engineering, Stanford University, Stanford, CA, 94305

*Author to whom correspondence should be addressed (wag@wag.caltech.edu)

## Supporting Information

### 1. Pseudopotentials and basis sets

The pseudopotentials used in these calculations are standard norm-conserving, non-separable pseudopotentials.[1] The LDA potentials for Si and H were generated using the generalized norm-conserving pseudopotential method. [2] The PBE potentials were generated using Hamann's new method for pseudopotentials. [3] The silicon pseudopotentials included up to $l$=2 projectors (with standard settings) and the $l$=2 potential was used as the local potential. The hydrogen atom was also treated as a pseudopotential

(rather than with a bare-core potential), with only an *l*=0 potential. Multiple tests with hydrogen atoms, $H_2$ molecules and water molecules verified that the energetics of the bare core hydrogen potential and the hydrogen pseudopotential are almost indistinguishable.

The basis functions are double-zeta plus polarization quality, formed from contracted Gaussians. Hence the Si-*s* and Si-*p*, and the H-*s* have two radial degrees of freedom, and the Si-*d* and H-*p* angular polarization have only one. The PBE basis for Si is a contracted (4s3p1d/2s2p1d) basis, the LDA Si basis is (4s4p1d/2s2p1d), and both the LDA and PBE basis sets for hydrogen are contracted (4s1p/2s1p) basis sets. This nomenclature denotes, for H for example, that four Gaussian *s*-functions are contracted into two independent functions, and one Gaussian *p*-function is used as one independent radial degree of freedom. The *d*-functions are made up of the five pure *l*=2 functions, i.e., the *s*-combination is excluded. The Gaussians and contraction coefficients for hydrogen and silicon are listed in Tables S-1 and S-2.

***Table S-1:*** *Basis set for hydrogen. The Gaussian decay constants $\alpha$ (1/bohr$^2$), and associated contraction coefficients $c_\alpha$ for the contracted Gaussian basis functions (unnormalized).*

| **H** | **s-functions** | | | **p-function** | |
|---|---|---|---|---|---|
| | $\alpha_s$ | $c_\alpha$ (1st zeta) | $c_\alpha$ (2nd zeta) | $\alpha_p$ | $c_\alpha$ |
| **LDA** | 0.112827 | 0.104600 | 0.083940 | 1.20 | 1.0 |
| | 0.407007 | 0.399225 | 0.145755 | | |
| | 1.260443 | 0.394750 | 0 | | |
| | 4.553255 | 0.380096 | 0 | | |
| **PBE** | 0.102474 | 0.087388 | 0.075281 | 1.10 | 1.0 |
| | 0.372304 | 0.405344 | 0.120939 | | |
| | 1.230858 | 0.485455 | 0 | | |
| | 4.783324 | 0.397563 | 0 | | |

***Table S-2:*** *Basis set for silicon. The Gaussian decay constants $\alpha$ (1/bohr$^2$), and associated contraction coefficients $c_\alpha$ for the contracted Gaussian basis functions (unnormalized).*

| Si | s-functions | | | p-functions | | | d-function | |
|---|---|---|---|---|---|---|---|---|
| | $\alpha_s$ | $c_\alpha$ (1st zeta) | $c_\alpha$ (2nd zeta) | $\alpha_p$ | $c_\alpha$ (1st zeta | $c_\alpha$ (2nd zeta) | $\alpha_d$ | $c_\alpha$ |
| **LDA** | 0.109463 | 0.335647 | 1.0 | 0.077837 | 0.0395395 | 1.0 | 0.4604 | 1.0 |
| | 0.294700 | 0.501166 | 0 | 0.227532 | 0.212571 | 0 | | |
| | 1.301011 | -1.026687 | 0 | 0.565609 | 0.242187 | 0 | | |
| | 2.602030 | 0.398914 | 0 | 1.131240 | -0.174847 | 0 | | |
| **PBE** | 0.104600 | 0.209953 | 1.0 | 0.094241 | 0.067616 | 1.0 | 0.45 | 1.0 |
| | 0.272263 | 0.559782 | 0 | 0.317679 | 0.318212 | 0 | | |
| | 1.300508 | -0.991282 | 0 | 1.561145 | -0.066383 | 0 | | |
| | 2.601030 | 0.334871 | 0 | | | | | |

**2. Slab model calculations**

Table S-3 contains the surface energy results for slab models of the 2x3H3T4 surface containing varying numbers of bulk layers, ranging from 2 to 14, and varying number of *fixed* bulk layers. All models were terminated on the bottom surface with a layer of fixed hydrogen atoms.

The results show that the surface energy calculations where all bulk layers are allowed to relax during the geometry optimization are the ones that most closely approach the value of the converged surface energy, and that six bulk layers are sufficient to obtain an accuracy better than 0.028 eV/1x1 cell. Since this convergence error is common to all models, it should not affect the relative energy differences between them.

***Table S-3:*** *Calculated surface energy (eV/1x1 cell) for the 2x3H3T4 surface using slab models with varying numbers of bulk layers and with varying numbers of fixed bulk layers. All models were terminated with a layer of fixed hydrogen atoms on the bottom surface. These results are depicted in Figure 4* ***of the paper****.*

| Total bulk layers | No bulk layers fixed | 2 bulk layers fixed | 4 bulk layers fixed | 6 bulk layers fixed |
|---|---|---|---|---|
| **2** | 1.483 | 1.667 | N/A | N/A |
| **4** | 1.228 | 1.324 | 1.415 | N/A |
| **6** | 1.184 | 1.197 | 1.267 | 1.354 |
| **8** | 1.170 | 1.215 | 1.226 | 1.296 |
| **10** | 1.164 | 1.169 | 1.226 | 1.238 |
| **14** | 1.156 | 1.159 | 1.159 | 1.162 |

### 3. Comparison of PBE and LDA surface energies

Table S-4 compares the surface energies obtained using the PBE and LDA approximations for cell sizes up to 3x3. The results show that the LDA values are consistently higher than the PBE values with an average difference of 0.152.

***Table S-4:*** *Comparison of LDA and PBE surface energies for a selected group of surfaces. All energies are in eV/1x1 cell.*

| Surface | PBE surface energy, eV/1x1 | LDA surface energy, eV/1x1 cell | LDA – PBE difference, eV/1x1 cell |
|---|---|---|---|
| **1x1 relaxed** | 1.200 | 1.451 | 0.250 |
| **√3x√3H3** | 1.360 | 1.487 | 0.127 |
| **√3x√3T4** | 1.110 | 1.240 | 0.130 |
| **2x2H3** | 1.209 | 1.322 | 0.114 |

| | | | |
|---|---|---|---|
| **2x2T4** | 1.084 | 1.200 | 0.116 |
| **DAS3x3** | 1.070 | 1.241 | 0.172 |

## 4. Comparison of PBE DFT Si(111) surface energies to published values from empirical and semi-empirical calculations

Table S-5 compares the ab initio surface energies obtained from our PBE DFT calculations to previously reported empirical and semi-empirical results. Our results are in qualitative agreement with those of Takahashi et al.[4] and Zhao et al.[5], who used a modified embedded atom model and a building block energy contribution model, respectively.

***Table S-5:*** *Comparison of PBE-DFT surface energy for Si(111) surfaces with published results from empirical or semi-empirical methods. The reference energy is zero for the bulk crystal unless otherwise indicated, in which case it is the relaxed 1x1 unreconstructed surface. Energies are in eV/1x1 cell.*

| **Surface** | **This work (*ab initio*)** | **Empirical surface energy, eV/1x1 cell** | | | | |
|---|---|---|---|---|---|---|
| | | **Takahashi et al. (1999)[4]** | **Zhao et al. (1998)[5]** | **Mercer and Chou (1993)[6]** | **Khor and Das Sarma (1989)[7]** | **Qian and Chadi (1987) [8,9]** |
| **Method** | PBE-DFT | MEAM[a] | BBEC[b] | TB[c] | MD[d] | TB[c] |
| **1x1 unrelaxed** | 1.224 | | | 1.131 | 0 (ref.)[e] | 0 (ref.) [e] |
| **1x1 relaxed** | 1.200 | | | 1.1 | -0.17 | -0.17 |
| **√3x√3H3 hex.** | 1.353 | | | | -0.075 | |
| **√3x√3T4 hex.** | 1.102 | | | 0.860 - 1.338 | -0.285 | |
| **2x2H3 hex.** | 1.209 | | | | -0.20 | |
| **2x2T4 hex.** | 1.083 | | | 0.790 - 1.198 | -0.25 | |
| **2x2H3 rect.** | 1.264 | | | | -0.166 | |
| **2x2T4 rect.** | 1.085 | | | | | |
| **2x3H3T4** | 1.184 | | | | | |

| | | | | | | |
|---|---|---|---|---|---|---|
| **C2x8** | 1.184 | | | 0.780 - 1.189 | | -0.180 |
| **DAS3x3** | 1.070 | 1.243 | 1.196 | | -0.326 | |
| **DAS5x5** | 1.048 | 1.211 | 1.168 | 0.729 – 1.143 | -0.344 | -0.395 |
| **DAS7x7** | 1.044 | 1.206 | 1.153 | 0.728 – 1.138 | -0.335 | -0.403 |
| **DAS9x9** | 1.055 | 1.226 | 1.164 | | -0.325 | -0.155 |

[a]Modified embedded atom model
[b]Building block energy contributions
[c]Tight binding model
[d]Molecular dynamics
[e]Absolute energies not provided

## 5. Spin states

Table S-6 contains the calculated high-spin surface energies for non-DAS surface structures. The results show that the for the 1x1, √3x√3H3 and √3x√3T4 surfaces, the lowest energy state has a net spin of one. For all other non-DAS structures the lowest energy state has no net spin. Tables S-7, S-8 and S-9 contain the calculated surface energies for the DAS 3x3, DAS 5x5 and DAS 7x7 surfaces for different numbers of unpaired electrons (spin polarization), including zero. All models contained six bulk layers and were terminated with a layer of fixed hydrogen atoms on the bottom surface. The lowest surface energy was obtained for spin zero and increased monotonically with increasing spin polarization. Figures S-1 and S-2 depict the results of tables S-7 and S-9 (the results of table S-8 are shown graphically in Figure 5 of the paper).

***Table S-6:*** *Calculated high-spin surface energy for non-DAS surface structures with respect to the zero spin state.*

| Surface | Spin Polarization | Surface energy, eV/1x1 cell |
|---|---|---|
| **1x1 unrelaxed** | 1 | -0.129 |
| **1x1 relaxed** | 1 | -0.106 |

| | | |
|---|---|---|
| **√3x√3H3 hex.** | 1 | -0.007 |
| **√3x√3T4 hex.** | 1 | -0.008 |
| **2x2H3 hex.** | 2 | 0.012 |
| **2x2T4 hex.** | 2 | 0.068 |
| **2x2H3 rect.** | 2 | -0.002 |
| **2x2T4 rect.** | 2 | 0.051 |
| **2x3H3T4** | 2 | 0.008 |
| **c2x8** | 4 | 0.001 |

***Table S-7:*** *Calculated surface energy for the DAS 3x3 surface as a function of the spin polarization, with respect to the singlet state. These results are shown graphically in Figure S-1.*

| Spin polarization | Surface energy, eV/1x1 cell |
|---|---|
| **0** | 0 |
| **1** | 0.011 |
| **2** | 0.019 |

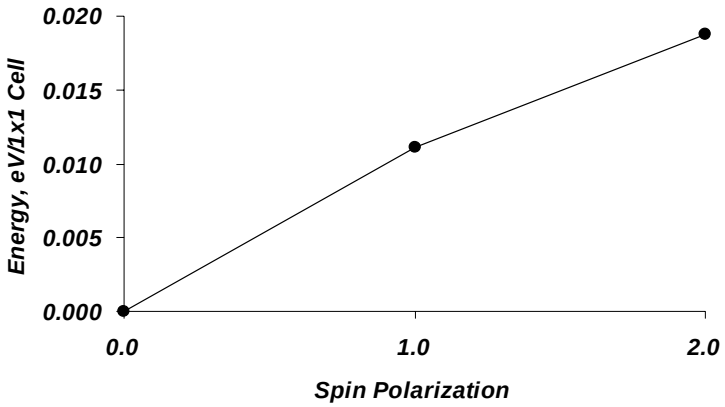


**Figure S-1.** Calculated surface energy of the DAS 3x3 surface as a function of the spin polarization, with respect to the singlet state (Table S-7). Note: the DAS 3x3 surface contains 2 dangling bonds.

***Table S-8:*** *Calculated surface energy for the DAS 5x5 surface as a function of the spin polarization, with respect to the singlet state. These results are shown graphically in Figure 6* ***of the paper****.*

| **Spin polarization** | **Relative surface energy, eV/1x1 cell** |
|---|---|
| **0** | 0 |
| **1** | $< 10^{-3}$ |
| **2** | 0.001 |
| **3** | 0.003 |
| **4** | 0.011 |
| **5** | 0.013 |
| **8** | 0.029 |

***Table S-9:*** *Calculated surface energy for the DAS 7x7 surface as a function of the spin polarization, with respect to the singlet state. These results are shown graphically in Figure S-2.*

| **Spin polarization** | **Relative surface energy, eV/1x1 cell** |
|---|---|
| **0** | 0 |
| **1** | $< 10^{-3}$ |
| **2** | $< 10^{-3}$ |
| **3** | $< 10^{-3}$ |
| **4** | $< 10^{-3}$ |
| **5** | 0.001 |
| **19** | 0.029 |

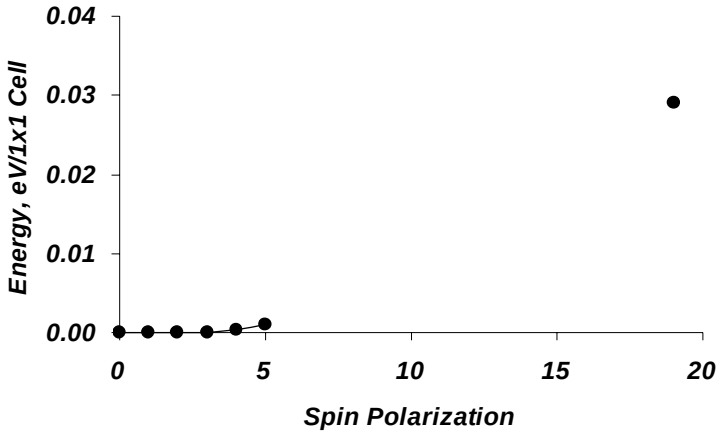


***Figure S-2:*** *Calculated surface energy of the DAS 7x7 surface as a function of the spin polarization, with respect to the singlet state (table S-9). Note: the DAS 7x7 surface contains 19 dangling bonds.*

**6. Comparison of 2x2 hexagonal and rectangular surfaces**

Tables S-10 and S-11 provide a comparison of the surface energy, sub-surface strain energy and adatom snap bond energy (as defined in section 4.2 of the paper), and adatom geometry for hexagonal and rectangular 2x2H3 and 2x2T4 surfaces. The results show that the surface energy is significantly different between the hexagonal and rectangular structures for the 2x2H3 surface, but not for the 2x2T4 surface. The surface energy of the 2x2H3 surface is ~0.22 eV/2x2 cell higher for the rectangular surface, primarily due to lower adatom bond energy (Table S-10). A Mulliken populations analysis of these surfaces (Figures S-3 and S-4) shows that there is significant charge separation in both cases, but that the geometry of the hexagonal cell allows this separation to remain local (thus providing an overall uniform charge distribution when many cells are considered), while the rectangular cell exhibits charge separation between infinite parallel lines in the green ($3^{rd}$) layer (again considering an infinite number of unit cells), with non-uniform charge distribution around the $2^{nd}$ layer dangling bond atoms (brown), thus leading to a less favorable energy. Figures S-5 and S-6 show that charge separation also takes place for the 2x2T4 rectangular surface in a

similar way, but that the charge distribution remains more uniform in the green layer (except for the green atom directly below the adatom). The adatom in the 2x2T4 rectangular surface can be stabilized by the 3rd layer (green) atom directly below it, which allows the 3rd layer atoms surrounding a 2nd layer dangling bond atom (brown) to all have the same charge and provide a more uniform charge distribution, similar to that of the hexagonal surface, leading to a negligible energy difference between the two surface structures.

***Table S-10:*** *2x2H3 hexagonal and rectangular electronic structure and geometry calculations. All energies are in eV per 2x2 unit cell.*

| | **HEX** | **RECT** | **RECT – HEX difference** |
|---|---|---|---|
| **Surface energy** | 4.838 | 5.058 | 0.220 |
| **Surface strain energy (below adatom)** | 0.883 | 0.804 | -0.079 |
| **Stabilization due to adatom snap bond energy** | -6.399 | -6.100 | 0.299 |
| **Adatom bond angle, degrees** | 85.4 | 85.5 | 0.1 |
| **Adatom bond length** | 2.61 | 2.60 | -0.01 |

***Table S-11:*** *2x2T4 hexagonal and rectangular electronic structure and geometry calculations. All energies are in eV per 2x2 unit cell.*

| | **HEX** | **RECT** | **RECT – HEX difference** |
|---|---|---|---|
| **Surface energy** | 4.333 | 4.341 | 0.008 |
| **Surface strain energy (below adatom)** | 0.798 | 0.923 | 0.125 |
| **Stabilization due to adatom snap bond energy** | -6.819 | -6.936 | -0.117 |
| **Adatom bond angle, degrees** | 94.7 | 94.1 | -0.6 |
| **Adatom bond length** | 2.49 | 2.47 | -0.02 |

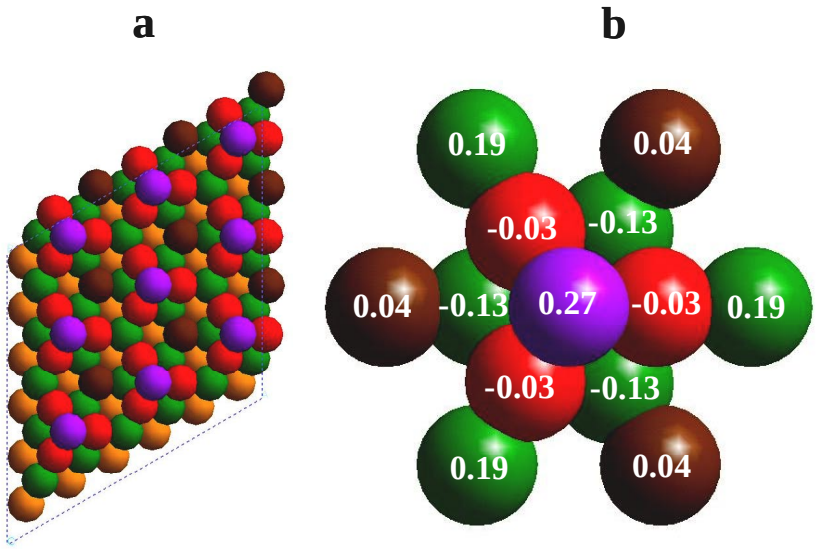


**Figure S-3.** 2x2H3 hexagonal surface partial atomic charges from Mulliken populations analysis. The results show significant charge separation in the unit cell, but the hexagonal symmetry allows the overall charge distribution to be uniform when large surface regions are considered.

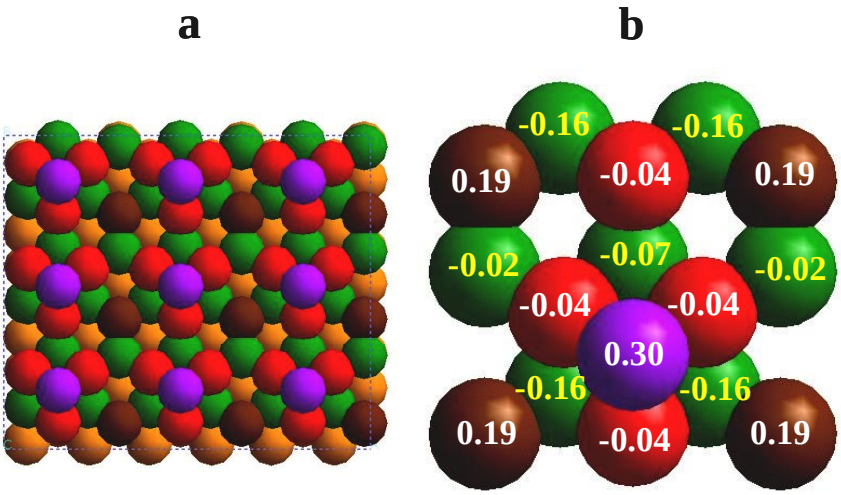

**Figure S-4.** 2x2H3 rectangular surface partial atomic charges from Mulliken populations. The results indicate that charge separation takes place in the 3rd layer (green with charge values highlighted in yellow) in a non-uniform manner, leading to dipoles between infinite parallel lines oriented with the size of the unit cell. This surface also has uneven charge distribution around the 2nd layer dangling bond atoms (brown).

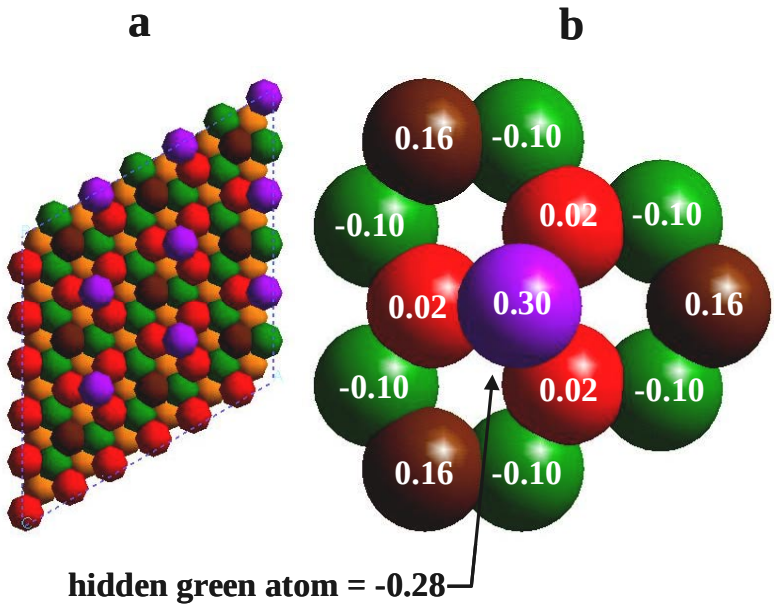


**Figure S-5.** 2x2T4 hexagonal surface partial atomic charges from Mulliken populations analysis. As with the 2x2H3 hexagonal surface, this structure shows significant charge separation in the unit cell, but the cell symmetry allows the overall charge distribution to be uniform when large surface regions are considered.

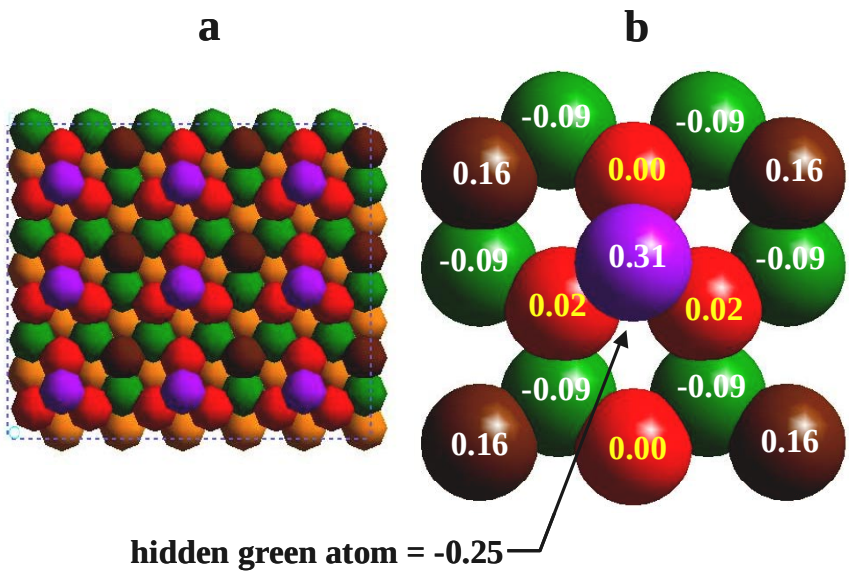


**Figure S-6.** 2x2T4 rectangular surface partial atomic charges from Mulliken populations analysis. The results show a nearly uniform charge distribution in the 2nd layer (red with charges highlighted in yellow), and also in the green layer (except for the atom directly below the adatom).

## 8. References


1. A. Redondo, W.A. Goddard III and T.C. McGill, Phys. Rev. B 15, 5038 (1977)
2. D.R. Hamann, Phys. Rev. 40, 2980 (1989)
3. D.R. Hamann, unpublished
4. K. Takahashi, C. Nara, T. Yamagishi and T. Onzawa, Appl. Surf. Sci. 151, 299 (1999)
5. Y.F. Zhao, H.Q. Yang, J.N. Gao, Z.Q. Xue and S.J. Pang, Phys. Rev. B 58 13824 (1997)
6. J.L. Mercer Jr. and M.Y. Chou, Physical Review B 48, 5374 (1993)

7. K.E. Khor and S. Das Sarma, Phys. Rev. B 40, 1319 (1989)

8. G.X. Qian and D.J. Chadi, J. Vac. Sci. Technol. B 5, 1079 (1986)

9. G.X. Qian and D.J. Chadi, J. Vac. Sci. Technol. A 5, 906 (1987)